SYNTHETIC SEISMOGRAMS IN TRANSVERSELY ISOTROPIC PLANE LAYERED MEDIA

C. GUENNOU

Université de Bretagne occidentale[1]

SISMOGRAMMES SYNTHÉTIQUES DANS LES MILIEUX STRATIFIÉS PRÉSENTANT UNE ISOTROPIE PLANE

Le but des présents travaux est de calculer la réponse des milieux stratifiés présentant une isotropie plane à l'excitation d'une source enterrée ou de surface, de façon à obtenir une méthode qui puisse aider à l'interprétation des sismogrammes réels.

Le calcul exposé ici, dans un domaine de fréquence f et de nombre d'onde k, est basé sur la méthode de réflexion de Kennett. Les déplacements dans l'espace et dans le temps sont calculés par une intégration numérique (transformée de Fourier-Hankel) de la réponse en fréquence et en nombre d'onde. La réponse numérique de surface d'un demi-espace à isotropie plane et à deux marqueurs excités par une source de surface est ici présentée. Les propriétés mécaniques du demi-espace proposé correspondent à celles de la gamme des sédiments marins. La fréquence et le décalage du domaine proposé correspondent à ceux employés dans la prospection géotechnique. Les effets de l'anisotropie sont mis en avant en comparant les réponses de l'exemple anisotrope à celles de l'exemple isotrope.

SYNTHETIC SEISMOGRAMS IN TRANSVERSELY ISOTROPIC PLANE LAYERED MEDIA

The purpose of the work presented in the paper, is to compute the response of transversely isotropic plane layered media excited by a buried or surface source, in order to obtain a method which can help interpreting real seismograms.

The computation in frequency f and wavenumber k domain based on the Kennett's reflectivity method is exposed. Displacements in space and time are calculated by numerical integration (Fourier-Hankel transform) of the response in frequency and wavenumber domain. The numerical surface response of a transverse isotropic two-layered half space excited by a surface source is presented. The mechanical properties of the proposed two-layered halfspace falls within the range of marine sediments. The frequency and offset proposed domain correspond with geotechnical surveys. Effects of anisotropy are put forward by comparing the responses in anisotropic case to the responses in isotropic case.

SISMOGRAMAS SINTÉTICOS EN MEDIOS DE ESTRATIFICACIÓN PLANA TRANSVERSALMENTE ISOTRÓPICOS

El objetivo del trabajo presentado en este artículo es computar la respuesta de medios de estratificación plana transversalmente isotrópicos cuando son estimulados por una fuente bajo tierra o superficial con el fin de obtener un método que pueda ayudar a interpretar sismogramas reales.

(1) 16 avenue Le Gorgeu, 29200 Brest - France

Se presenta el cómputo en el ámbito de la frecuencia f y del número de onda k en base al método de reflectividad de Kennett. Los desplazamientos en el espacio y en el tiempo son calculados mediante integración numérica (transformación de Fourier-Hankel) de la respuesta en el ámbito de la frecuencia y del número de onda. Se presenta la respuesta superficial numérica de un semi-espacio de dos capas transversalmente isotrópico estimulado por una fuente superficial. Las propiedades mecánicas del semi-espacio de dos capas propuesto queda comprendido dentro del rango de los sedimentos marinos. El ámbito de frecuencia y de compensación propuesto corresponde al de las prospecciones geotécnicas. Se destacan los efectos de la anisotropía comparando las respuestas en un caso anisotrópico con las respuestas en un caso isotrópico.

INTRODUCTION

Offshore geotechnical engineers are in a crucial need of knowledge of marine sediments properties. Technical tools exist which can provide accurate seismic informations. The gap is now between acquisition and interpretation. Direct and inverse modelling are therefore the only tools that can help in this way. Therefore two approaches are needed.

– Experimental approach: seismic wave experiments on the sea floor, performed at a very specific scale corresponding to geotechnical surveys are carried out (Krone, 1996, 1997). Seismic *SH*-waves are generated by applying a shear strain parallel to the sediment surface with an orientation perpendicular to the direction of propagation. Scholte waves are generated by applying a vertical strain to the sediment.
– Numerical approach: a seismogram computation code is developped. The computation is based on the Kennett's reflectivity method (Kennett 1983). Its main advantage is to allow the computation of the complete response of the layered medium to a point source, including all the free surface and interlayers multiples. It has been used in various applications (Booth, 1983; Fryer, 1984, 1986; Mallick, 1988; Meunier, 1990; Guennou, 1996).

Since marine sediments are strongly anisotropic (Bachman, 1979, 1983) and since anisotropy of marine sediments results mainly from bedding, marine sediments, as any lamellate medium (composed of different isotropic layers that are much thinner than a seismic wavelength), are supposed to exhibit transverse isotropy with an axis of symmetry orthogonal to the layering. So, in this paper, the Kennett's reflectivity method for computing seismograms is adapted to the study of marine sediments, by extending it in the case of tranverse isotropy. Within each solid layer, being a viscous linearly elastic homogeneous medium, the wavespeeds in directions perpendicular to the symmetry axis of the stratification (axis z) are all the same but differ from those parallel to the axis. The attenuation is handled with complex wave velocities. Fluid layers bounding or within the stratification can be taken into account.

1 THEORY

1.1 The Transversely Isotropic Homogeneous Medium

In the absence of sources, the incremental displacement u, induced by the propagation of a seismic wave in a homogeneous medium is governed by the equation of motion:

$$\rho \partial_{tt} u = \mathrm{div}\left[\sigma\right]$$

where ρ is the density of the medium, $[\sigma]$ the stress tensor, and ∂_{tt} the second derivative of the considered quantity with respect to time.

In a linearly elastic medium, under small perturbations, the relationship between the linearized strain tensor $[\varepsilon] = 1/2\ (\mathrm{grad}\ u + \mathrm{grad}^t\ u)$ and the stress tensor $[\sigma]$ is the following:

$$\left[\sigma\right] = \left[\tilde{C}\right]\left[\varepsilon\right]$$

where $[\tilde{C}]$ is the elastic modulus tensor. The latter tensor, in which each component is constant, completely characterizes the elasticity of the medium. Its simplest form arises for isotropic media.

For Transversely Isotropic media (axis z), the elastic modulus tensor $[\tilde{C}]$ has five independant components:

$$\left[\tilde{C}\right] = \begin{bmatrix} C_{11} & C_{12} & C_{13} & 0 & 0 & 0 \\ C_{12} & C_{11} & C_{13} & 0 & 0 & 0 \\ C_{13} & C_{13} & C_{33} & 0 & 0 & 0 \\ 0 & 0 & 0 & C_{44} & 0 & 0 \\ 0 & 0 & 0 & 0 & C_{44} & 0 \\ 0 & 0 & 0 & 0 & 0 & C_{66} \end{bmatrix}$$

with $C_{12} = C_{11} - 2C_{66}$.

A cylindrical set of coordinates (r, θ, z) is chosen. The displacement u may be represented in terms of its components:

$$u\,(r, \theta, z) = u_r\, e_r + u_\theta\, e_\theta + u_z\, e_z$$

using the orthogonal unit vectors e_r, e_θ, and e_z.

A set of combined variables for displacements and stresses is introduced in order to decouple *P*-, *SV*-waves and *SH*-waves:

$$\begin{aligned} u_V &= r^{-1}\left[\partial_r\left(r u_r\right) + \partial_\theta u_\theta\right] \\ u_H &= r^{-1}\left[\partial_r\left(r u_\theta\right) - \partial_\theta u_r\right] \\ \sigma_{Vz} &= r^{-1}\left[\partial_r\left(r \sigma_{rz}\right) + \partial_\theta \sigma_{\theta z}\right] \\ \sigma_{Hz} &= r^{-1}\left[\partial_r\left(r \sigma_{\theta z}\right) - \partial_\theta \sigma_{rz}\right] \end{aligned}$$

Indeed, by isolating the z derivatives in the equations of motion and in the equations characterizing the elasticity of the medium, we obtain six equations which are separated into two decoupled sets:

$$\begin{aligned} \partial_z u_V &= C_{44}^{-1}\,\sigma_{Vz} - \nabla_h\, u_z \\ \partial_z u_z &= C_{33}^{-1}\left(\sigma_{zz} - C_{13}\, u_V\right) \\ \partial_z \sigma_{Vz} &= \left[\rho \partial_{tt} - \left(C_{11} - C_{13}^2 C_{33}^{-1}\right)\nabla_h\right] u_V - C_{13} C_{33}^{-1} \nabla_h\, \sigma_{zz} \\ \partial_z \sigma_{zz} &= \rho \partial_{tt} u_z - \sigma_{Vz} \end{aligned}$$

$$\begin{cases} \partial_z u_H = C_{44}^{-1}\,\sigma_{Hz} \\ \partial_z \sigma_{Hz} = \left(\rho \partial_{tt} - C_{66}\,\nabla_h\right) u_H \end{cases}$$

where ∇_h is the horizontal Laplacian defined by:

$$\nabla_h f = r^{-1}\,\partial_r\left(r \partial_r f\right) + r^{-2} \partial_{\theta\theta} f$$

The first set couples *P* waves to *SV* shear waves. The second set includes only *SH* shear waves.

1.2 The Change of Domain

It is now convenient to operate a change of domain in order to transform partial derivative equations into ordinary second order differential equations. The change of domain is made by applying a Fourier transform with respect to time t, followed by a Hankel transform.

The latter transform allows a change of domain from polar coordinates (r, θ) to wavenumber k and azimuthal order m domain:

$$\tilde{f}(k, m) = \frac{1}{2\pi} \int_{r=0}^{+\infty} \int_{\theta=-\pi}^{+\pi} r\, J_m(k r)\, e^{-im\theta}\, f(r, \theta)\, \mathrm{d}r\, \mathrm{d}\theta$$

and satisfies the following property $\tilde{\nabla}_h\, f = -k^2\, \tilde{f}$.

For each azimuthal order *m*, the column vectors $B_{PSV} = (U, V, S, P)^t$ and $B_{SH} = (W, T)^t$ are introduced. *U, V, W, P, S, T* are variables related to the transforms of the new displacement and stress variables previously defined:

$$U = \bar{u}_z \quad ; \quad P = \omega^{-1}\,\tilde{\sigma}_{zz}$$
$$V = -k^{-1}\tilde{u}_V \quad ; \quad S = -(\omega k)^{-1}\,\tilde{\sigma}_{Vz}$$
$$W = -k^{-1}\tilde{u}_H \quad ; \quad T = -(\omega k)^{-1}\,\sigma_{Hz}$$

(ω is the circular frequency arising in the Fourier transform).

At last, if we work in terms of horizontal slowness $p = k/\omega$ rather than with the horizontal wavenumber *k*, the two transformed sets take a very convenient form:

$$\partial_z B_{PSV} = \omega\, \mathbb{A}_{PSV}\, B_{PSV},\ \partial_z B_{SH} = \omega\, \mathbb{A}_{SH}\, B_{SH}$$

where $\mathbb{A}_{PSV}$ and $\mathbb{A}_{SH}$ are respectively 4 x 4 and 2 x 2 matrices depending on the density, the elastic modulus of the medium and the horizontal slowness *p*, and defined by:

$$\mathbb{A}_{PSV} = \begin{bmatrix} 0 & p\dfrac{C_{13}}{C_{33}} & \dfrac{1}{C_{33}} & 0 \\ -p & 0 & 0 & \dfrac{1}{C_{44}} \\ -\rho & 0 & 0 & p \\ 0 & -\rho + p^2\left(C_{11} - \dfrac{C_{13}^2}{C_{33}}\right) & -p\dfrac{C_{13}}{C_{33}} & 0 \end{bmatrix}$$

$$\mathbb{A}_{SH} = \begin{bmatrix} 0 & \dfrac{1}{C_{44}} \\ -\rho + p^2 C_{66} & 0 \end{bmatrix}$$

From now on, we omit to precise the index *PSV* and *SH*, as the two decoupled problems *PSV* and *SH* are now easily solved by applying the same method.

We name *D* the eigenmatrix for *A* (see the mathematical annex for the analytical expression of the matrix *D*). The matrix *D* is independent of the depth *z* (*A* is independent of *z*), so the relation $\partial_z B = \omega AB$ is equivalent to:

$$\partial_z\,(\mathbb{D}^{-1}B) = \omega\,\mathbb{D}^{-1}\,\mathbb{A}\,B = \omega\,\Lambda\,(\mathbb{D}^{-1}B)$$

where $\Lambda = \mathbb{D}^{-1}\,\mathbb{A}\,\mathbb{D}$ is the diagonal matrix whose entries are the eigenvalues of $\mathbb{A}$ (see the mathematical appendix for the analytical expression of the eigenvalues of $\mathbb{A}$).

The components of vector $V = \mathbb{D}^{-1}\,B$ are the solutions of the latter equations. Each of these components might be interpreted as an upgoing or downgoing wave according to its dependency on the *z* coordinate.

1.3 The Reflectivity Method

Kennett's method relies on the continuity of the stress displacement vector *B* at any depth of the stratification. If we name z_+ the depth just below an interface and z_- the depth just above the same interface, the continuity of vector *B* at depth *z* allows us to write:

$$V(z_+) = (\mathbb{D}+)^{-1}\,\mathbb{D}-\,V(z_-)$$

or, by using the Kennett's notation:

$$\begin{pmatrix} V_U(z_+) \\ V_D(z_+) \end{pmatrix} = \begin{pmatrix} Q_{11} & Q_{12} \\ Q_{21} & Q_{22} \end{pmatrix} \begin{pmatrix} V_D(z_-) \\ V_U(z_-) \end{pmatrix}$$

where the indices *U* and *D* mean “up” and “down” for upgoing and downgoing waves.

By comparing the latter relationship to the following one introducing reflection (*R*) and transmission (*T*) coefficients of the interface:

$$\begin{pmatrix} V_U(z_-) \\ V_D(z_+) \end{pmatrix} = \begin{pmatrix} R_D(z_+, z_-) & T_U(z_+, z_-) \\ T_D(z_+, z_-) & R_U(z_+, z_-) \end{pmatrix} \begin{pmatrix} V_D(z_-) \\ V_U(z_+) \end{pmatrix}$$

we are able to relate the reflection transmission coefficients to the coefficients Q_{ij}.

In the isotropic case, for a suitable normalisation of eigenvectors, the analytical expression of the matrix $\mathbb{D}^{-1}$ is easily deduced from the analytical expression of matrix $\mathbb{D}$, and the reflection transmission coefficients are symmetrical (Kennett, 1978). This trick is conserved in the case of transverse isotropy.

We introduce the partitions of the matrix $\mathbb{D}$:

$$\mathbb{D} = \begin{pmatrix} M_U & M_D \\ N_U & N_D \end{pmatrix}$$

and the quantity:

$$\langle M_U, M_D \rangle = M_U^t\, N_D - N_U^t\, M_D$$

If we have $\langle M_U, M_D \rangle = iI$ (*PSV* - problem), where I is the identity matrix, and $\langle M_U, M_D \rangle = i$ (*SH*-problem), then:

$$D^{-1} = i \begin{pmatrix} -N_D^t & M_D^t \\ N_U^t & -M_U^t \end{pmatrix}$$

$$Q_{11} = Q_{22} = i \left\langle M_{D_-}, M_{U^+} \right\rangle$$

$$Q_{12} = Q_{21} = i \left\langle M_{D_-}, M_{D^+} \right\rangle$$

$$R_D(z_+, z_-) = R_D^t(z_+, z_-) = Q_{12}\, Q_{11}^{-1}$$

$$R_U(z_+, z_-) = R_U^t(z_+, z_-) = -\, Q_{11}^{-1} Q_{12}$$

$$T_D(z_+, z_-) = T_U^t(z_+, z_-) = Q_{11}^{-1}$$

A recursive algorithm allows us to generate a propagator matrix that relates the wave vectors at two different depths of the stratified medium.

The point source is introduced as a discontinuity of the stress-displacement vector B across the source plane (depth z_s). By using the matrix $\mathbb{D}^{-1}(z_s)$, an alternative approach is to consider the source as giving rise to a discontinuity across the source plane in the wavevector V.

The boundary conditions imposed on the seismic wavefield are: vanishing stresses at the free surface ($z = 0$), the half space is assumed to be uniform below depth z_L, and in this region, only downgoing waves are present.

The Ancalsis code computes, in the (f, k) domain, from the addition rules of reflection-transmission coefficients and the boundary conditions, the matrix relating the wavevector at receiver plane (depth z_r) to the discontinuity in the wavevector V across z_s. Stresses and displacements at receiver plane, are recovered by computing the product $\mathbb{D}(z_r)\, V(z_r)$. They depend on the azimuthal order m.

1.4 Recovery of the Response in Space and Time

The last step of the computation is to inverse the Fourier and the Hankel transforms in order to recover displacements and stresses at depth z_r in space and time. The computation of the m-order Hankel transform:

$$f_m(r) = \int_{k=0}^{+\infty} \tilde{f}(k)\, J_m(k r)\, k \, \mathrm{d}k$$

for $m \neq 0$, is solved by computing the equivalent combination of a m-order Abel transform and a Fourier transform. The m-order Abel transform is defined as:

$$A_m(f(k)) = g_m(y) = \int_{k=|y|}^{+\infty} \frac{2T_m(k) f(k)}{\sqrt{1 - \left(\frac{y}{k}\right)^2}} \mathrm{d}k$$

where $T_m(x) = \cos(m(a \cos x))$ is the Chebyshev polynomial of the first kind, order m. By using the development of functions T_m, the relationships between zero-order Abel transform and higher-order Abel transforms are obtained:

$$A_1(f(k)) = y\, A_0\left(\frac{f(k)}{k}\right)$$

$$A_2(f(k)) = 2y^2\, A_0\left(\frac{f(k)}{k^2}\right) - A_0(f(k))$$

The fast zero-order Abel transform algorithm described in Hansen (1985) is used in the Ancalsis code.

The inverse Fourier transform with respect to frequency f is computed, or not, after a convolution with a spectrum of a signal source. The time seismogram is then filtered.

2 RESULTS

2.1 The Chosen Data

Numerical seismograms are presented, in the case of a layer overlying an uniform half-space which mechanical properties are given in the Table 1.

The viscosity of the two-layered half space is taken into account by introducing complex wave velocities defined by:

$$V_{complex} = V_{real}(1 + 0.02i)$$

This example of stratified medium is very simple, it has been chosen on purpose to show the correctness of the computation. Nevertheless, the chosen velocities belong to the range of velocities appearing in Hamilton's studies about the geoacoustic modeling of the sea floor (Hamilton, 1980; Nolet, 1996).

TABLE 1

Parameters of the anisotropic model

TIV model	**Layer (5 meters depth)**	**Half space**
Density ρ	1200 kg/m^3	1500 kg/m^3
Vertical compressional velocity $V_{P,v} = \sqrt{C_{33}/\rho}$	1500 m/s	1700 m/s
Horizontal compressional velocity $V_{P,h} = \sqrt{C_{11}/\rho}$	1800 m/s	2200 m/s
Vertical shear velocity $V_{S,v} = \sqrt{C_{44}/\rho}$	400 m/s	560 m/s
Horizontal shear velocity $V_{S,h} = \sqrt{C_{66}/\rho}$	500 m/s	800 m/s
Additional velocity $\sqrt{C_{13}/\rho}$	1530 m/s	1500 m/s
Thomsen parameters		
$\varepsilon = \dfrac{C_{11} - C_{33}}{2C_{33}}$	0.220	0.337
$\gamma = \dfrac{C_{66} - C_{44}}{2C_{44}}$	0.281	0.520
$\delta = \dfrac{(C_{13} + C_{33})(C_{13} - C_{33} + C_{44})}{2C_{33}(C_{33} - C_{44})}$	0.122	-1.127

Figures 1 and 2 present the slownesses of *P*-, *SV*- and *SH*-waves within, respectively the upper layer and the half-space, as functions of the horizontal slowness *p*.

Figure 1 shows that, within the upper layer, the *SV*-wave velocity is smaller than the *SH*-wave velocity in all the directions of propagation (except the vertical direction).

Figure 2 shows that, within the uniform half-space, there is an other direction of propagation, different of the vertical direction, for which the *SV*- and *SH*-waves velocities are the same. And between this particular direction and the vertical direction, the *SV*- wave velocity is faster than the *SH*-wave velocity. Figures 1 and 2 obviously show the critical slownesses for *P*-, *SV*- and *SH*- waves in a vertical transverse isotropic medium which are respectively:

$$\frac{1}{V_{P.h}},\ \frac{1}{V_{S,v}} \text{ and } \frac{1}{V_{S,h}}$$

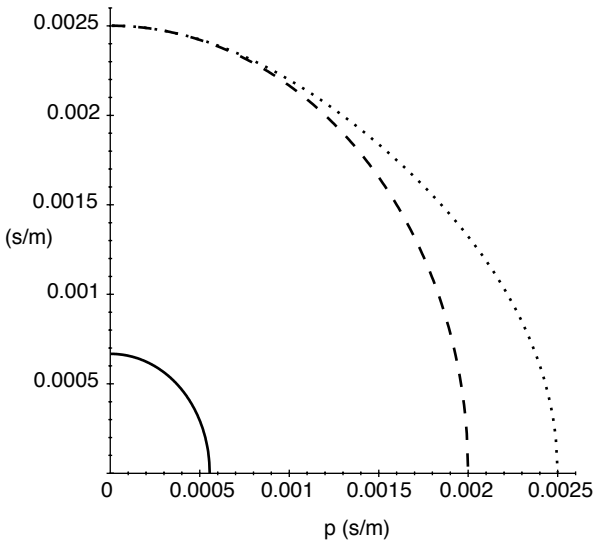

Figure 1

Slownesses of *P*-waves (solid line), *SH*-waves (dashed line) and *SH*-waves (dotted line) as functions of the horizontal slowness *p* within the upper layer.

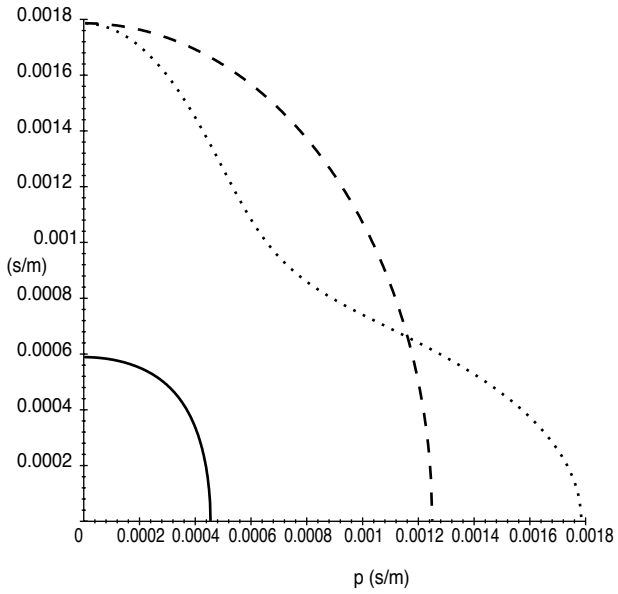

Figure 2

Slownesses of *P*-waves (solid line), *SH*-waves (dashed line) and *SV*-waves (dotted line) as functions of the horizontal slowness *p* within the half-space.

The source is assumed to be a point force, located at a point *S* on the surface of the stratification. The displacements are computed for points *R* such that:

$$\vec{SR} = n\,\Delta r\,e_r$$

where *n* is an integer, Δr the distance between two consecutive points, and $n\Delta r$ the variable called the "offset", that is to say the distance between a point *R* and the axis (*S*, e_z) perpendicular to the surface. A configuration of usual seismic experiments is then respected.

2.2 Intermediate Results: the Needed Reflection Coefficients

In this case, the one and only reflection coefficients needed for computing the complete surface response by using the reflectivity method, are the downgoing waves reflection coefficients at the one and only interface of the stratification. It is the reason why the latter coefficients, coming directly from the code, are discussed now, in order to validate them with respect to Daley 's work (Daley, 1977).

The reflection coefficient R_D^{SH-SH} as function of the horizontal slowness *p* simply increases (Fig. 3). The behaviour is simple and R_D^{SH-SH} is always real. Its amplitude reaches the value 1 at $p = 1/V_{S,h}^{(2)}$ (here 1.250 s/km, the critical slowness for *SH*-waves in the half-space), and keeps the value 1 for $p > 1/V_{S,h}^{(2)}$.

The behaviour of the reflection coefficients relative to the coupled *P-SV* system is more complicated (Fig. 4a, 4b, 4c, 4d).

At vertical incidence, there is neither conversion from *P* to *SV*-waves nor conversion from *SV*- to *P*-waves.

For $p < 1/V_{P,h}^{(2)}$ (0.455 s/km in the example, critical slowness for the *P*-wave in the half-space) all the reflection coefficients for the *P-SV* system are real. For $1/V_{P,h}^{(2)} < p < 1/V_{P,h}^{(1)}$, they are all complex.

At $p = 1/V_{P,h}^{(1)}$ (0.556 s/km, critical slowness for *P*-waves in the upper layer), the *P*-waves are travelling horizontally in the upper layer and the coefficient R_D^{P-SV} drops to the real value 0 and the coefficient R_D^{P-P} reaches to real value 1.

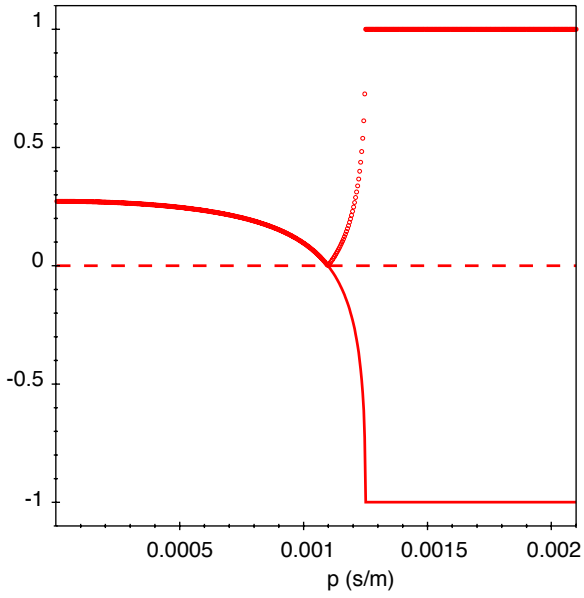

Figure 3

Coefficient R_D^{SH-SH} at the interface as a function of the horizontal slowness *p*, (solid line: real part, dashed line: imaginary part, dotted: amplitude).

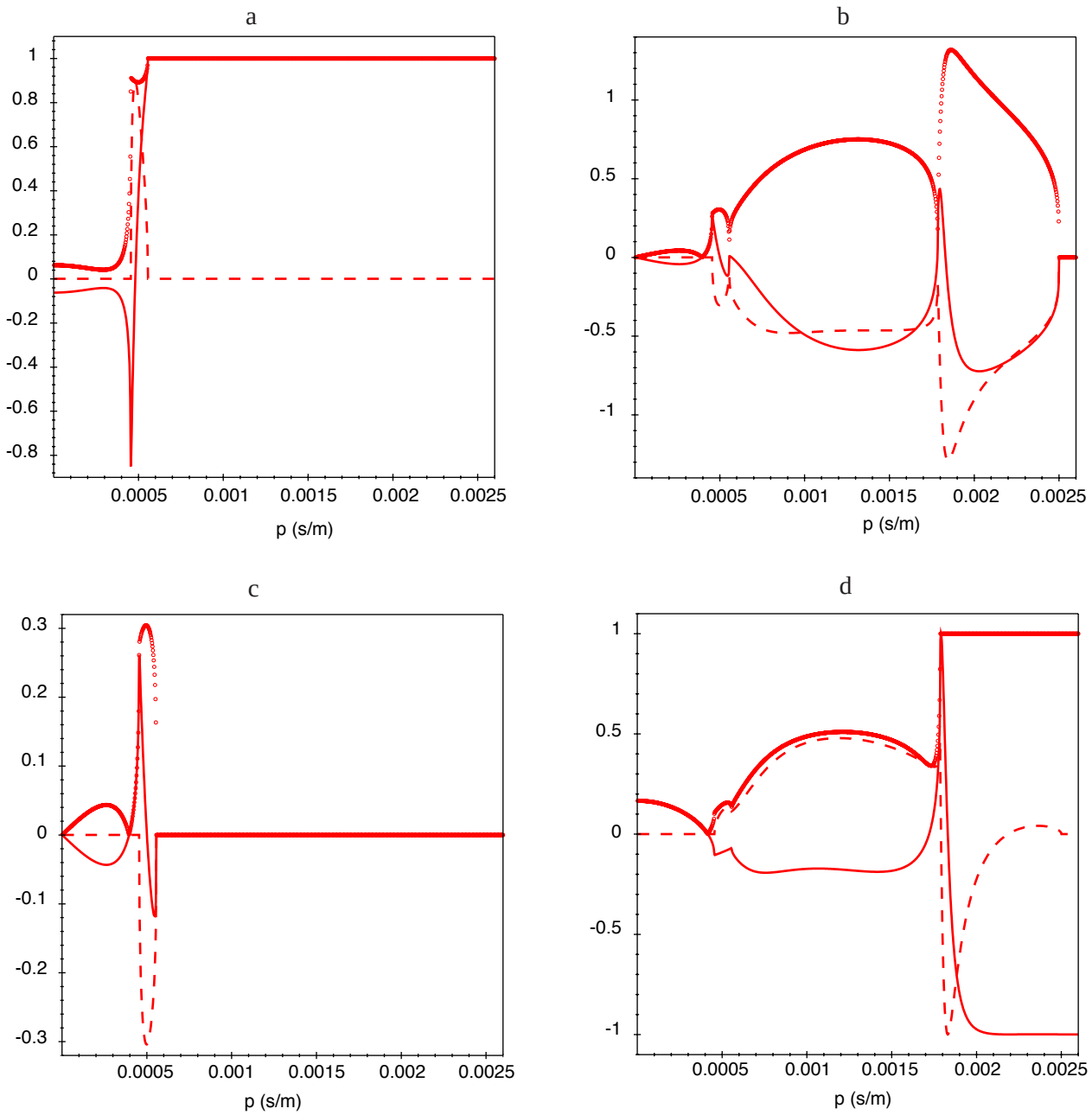

Figure 4

Coefficients : (a) R_D^{P-P}, (b) R_D^{SV-P}, (c) R_D^{P-SV} and (d) R_D^{SV-SV} at the interface as functions of horizontal slowness p, (solid line = real part, dashed line = imaginary part, dotted = amplitude).

The coefficients R_D^{SV-P} and R_D^{SV-SV} are highly influenced by the *P*-wave behaviour, the real and imaginary parts of these coefficients have an inflexion at critical slownesses of *P*-waves.

The curves of the real and imaginary parts of the coefficient R_D^{SV-P} also exhibit an inflexion point for (1.786 s/km, critical slowness for *SV*-wave in the half-space), and for p larger than this value, the amplitude of R_D^{SV-SV} is equal to 1.

At last, at $p = 1/V_{S,v}^{(1)}$ (2.500 s/km, critical slowness for the wave in the upper layer), the *SV*-wave travels horizontally in the upper layer and the coefficient R_D^{SV-P} drops to the real value 0 and the coefficient R_D^{SV-SV} reaches to the real value 1.

2.3 Numerical Seismograms: Effect of Anisotropy

By using only an analysis of velocities, there are two ways for observing the effects of transverse isotropy on seismograms. The first way is to compute the displacements for different directions of propagation. It is possible, in particular when source and receiver horizontal plane are not at the same depth.

When source and receivers are at the same depth, at the surface for example (as it was the case during the *Ifremer* seismic waves experiments, and as it is the case for the presented synthetic seismograms), the one and only direction between source and receivers is horizontal. Although, the effects of anisotropy can be observed by changing the direction of the source force. When the point force is horizontal and equal to $F_\theta\, e_\theta$, only the *SH*-waves are generated, only the orthoradial displacements u_θ do not vanish (Fig. 5). When the point force is vertical, located at the surface, *P*- and *SV*-waves are generated, and there are no orthoradial displacements.

Two examples of numerical seismograms are presented:

– The first one (Fig. 7a), is the radial response, in the (f, k) domain, at the surface of the two-layered medium excited by a vertical point force $F_z e_z$, placed at the surface. The surface wave (Rayleigh wave) and *SV*-waves are observed. The Rayleigh wave velocity is slightly slower than the *SV*-wave velocity. The *P*-waves are also present, but their amplitude are insignificant. They can be observed when their attenuation is very small compared with the shear wave attenuation.

– The second one (Figs 7b and 5), is the orthoradial response, respectively in the (f, k) domain and in space and time, at the surface, of the two-layered medium excited by a horizontal point force $F_\theta\, e_\theta$, always placed at the surface.

Figure 7b shows the Love wave dispersion curves. The classical results about Love wave propagation can be observed:

– the Love wave velocity v is restricted to

$$V_{S,h}^{(1)} < v < V_{S,h}^{(2)}$$

– the successive modes of Love waves have a lower cutoff in frequency;

– at high frequencies, the Love wave dispersion curves have the asymptotic value $V_{S,h}^{(1)}$.

Figure 5 shows the temporal numerical seismogram, not filtered in frequency, directly obtained by applying a numerical inverse Fourier-Hankel transform to the results in frequency and wavenumber domain. The traces are normalized.

The latter numerical seismograms are compared to those (Figs 6a and 6b), obtained in the isotropic case (the geometry of stratification and localisation of source and receivers are identical) (Table 2).

One of the primary effects of transverse isotropy can be observed with a simple analysis of velocities.

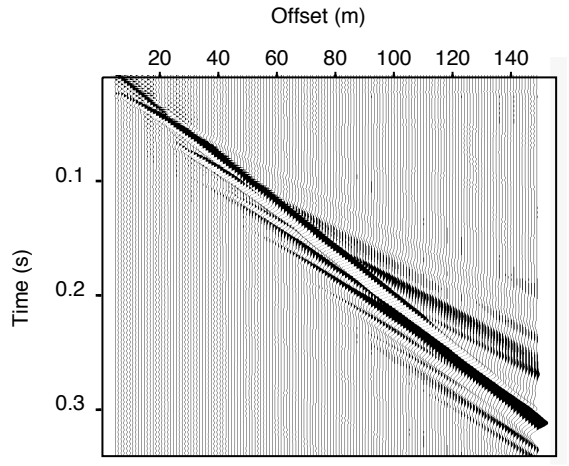

Figure 5

Orthoradial displacements, in time and space, at the free surface of the two-layered half-space excited by a surface source (source = horizontal force $F_\theta e_\theta$).

TABLE 2

Parameters of the isotropic model

Isotropic model	Layer (5 meters depth)	Half-space
Density γ	1200 kg/m^3	1500 kg/m^3
Compressional velocity $V_P = \sqrt{C_{33}/\rho}$	1500 m/s	1700 m/s
Shear velocity $V_S = \sqrt{C_{44}/\rho}$	400 m/s	560 m/s

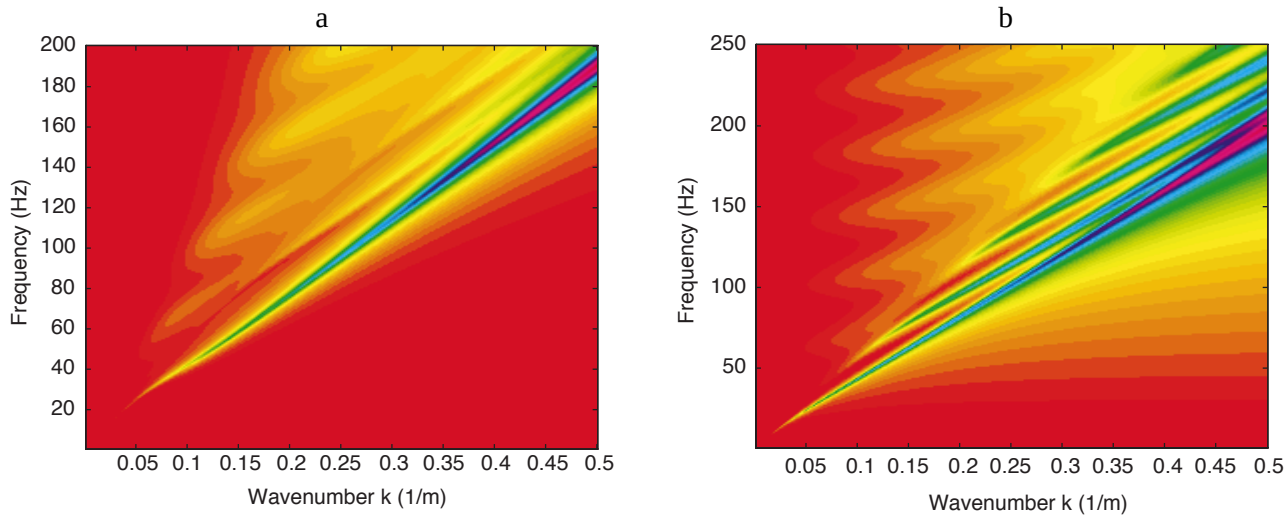

Figure 6

Radial displacement (source = vertical force $F_z e_z$) (a) and orthoradial displacement (source = horizontal force $F_\theta e_\theta$) (b), in the frequency and wavenumber domain, at the free surface of the two-layered half-space (isotropic model) excited by a surface located at the surface.

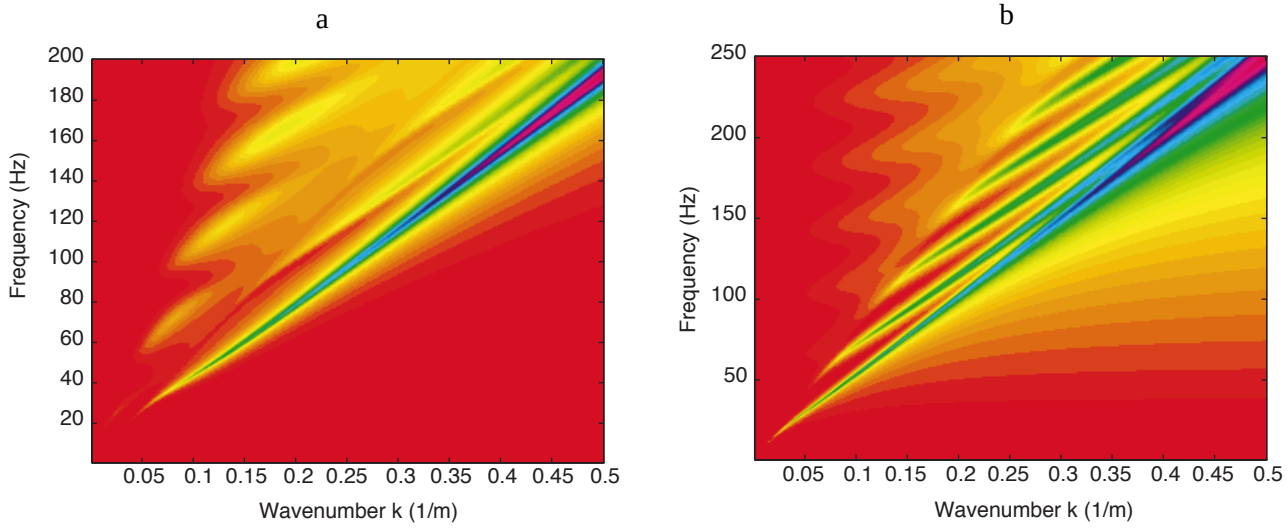

Figure 7

Radial displacement (source = vertical force $F_z e_z$) (a) and orthoradial displacement (source = horizontal force $F_\theta e_\theta$) (b), in the frequency and wavenumber domain, at the free surface of the two-layered half-space (TIV model) excited by a surface located at the surface.

In the anisotropic case there is a difference between the velocity of shear waves generated with a vertical point force and velocity of shear waves generated with a horizontal point force. This difference is a mesure of anisotropy recovered in the Thomsen parameter γ. Of course, in the isotropic case, this difference vanishes.

CONCLUSION

One key-point in interpreting *S*-wave seismograms, recorded in shallow waters at very high resolution (mean frequency 200 Hz) is to recognize incoming surface waves, and to distinguish dispersion due either to guided propagation modes or to viscoelaticity.

The seismogram computation code, presented in this paper, was validated using specific scale corresponding to geotechnical surveys. Therefore it provides a unique tool for interpreting real seismograms in the domain of offshore geotechnical engineering.

REFERENCES

Bachman R.T. (1979) Acoustic anisotropy in marine sediments and sedimentary rocks. *J. Geophys. Res*., 84.

Bachman R.T. (1983) Elastic anisotropy in marine sedimentary rocks. *J. Geophys. Res*., 88.

Booth D.C. and Crampin S. (1983) The anisotropic reflectivity technique: theory. *Geophys. J. Roy. Astr. Soc.*, 72.

Daley P.F. (1977) Reflection and transmission coefficients for transversely isotropic media. *Master Thesis*, Departement of Physics, University of Alberta, Edmonton.

Fryer G.J. and Frazer L.N. (1984) Seismic waves in stratified anisotropic media. *Geophys. J. Roy. Astr. Soc*., 78.

Fryer G.J. and Frazer L.N. (1987) Seismic waves in stratified anisotropic media-II. Elastodynamic eigensolutions for some anisotropic system. *Geophys. J. Roy. Astr. Soc.*, 91.

Guennou C. and Meunier J. (1996) Computation of seismograms in frequency and wave number domain. *Soc. Expl. Geoph.*, Denver, USA.

Guust N. and Leroy M.D. (1996) Waveform analysis of Scholte modes in ocean sediment layers. *Geophys. J. Int*., 25.

Hamilton E.L. (1980) Geoascoutical modeling of the sea floor. *J. Acoust. Soc. Am*., 68.

Hansen E.W. (1985) Fast Hankel Transform Algorithm. *IEEE Transactions on Acoustics, Speech, and Signal Processing*, ASSP-33, number 3.

Kennet B.L.N., Kerry N.J. and Woodhouse J.H. (1978) Symmetries in the reflection and transmission of elastic waves. *Geophys J. R. Astr. Soc.*, 52.

Kennett B.L.N. and Kerry N.J. (1979) Seismic waves in a stratified half space. *Geophys J. R. Astr. Soc.*, 57.

Kennett B.L.N. (1980) Seismic waves in a stratified half space-II. Theoretical seismograms. *Geophys J. R. Astr. Soc.*, 61.

Kennett B.L.N. (1983) *Seismic Wave Propagation in Stratified Media*, Cambridge University Press.

Krone R., Guennou C. and Theilen F. (1996) Shallow water profiling. *European Association of Exploration Geophysicists*, Amsterdam.

Krone R. (1997) Sismique onde S en faible profondeur d'eau: propriétés de cisaillement des sédiments marins superficiels par inversion simultanée de la dispersion des ondes de Love et de Sholte. *Ph.D Thesis*, University of Bretagne occidentale.

Mallick S. and Frazer L.N. (1988) Rapid computation of multioffset vertical seismic profile synthetic seismograms for layered media. *Geophysics*, 53

Meunier J. and Guennou C. (1990) Computation of shear waves by integral equation methods in stratified media. *Shear Waves in Marine Sediment, La Spezia, Italy.*

Final manuscript received in July 1998

Mathematical Appendix

1 EIGENVALUES FOR $\mathbb{A}$

1.1 PSV Propagation

The four eigenvalues are :
$-i\gamma_P$ (upgoing *P*-wave), $-i\gamma_{SV}$ (upgoing *SV*-wave), $i\gamma_P$ (downgoing *P*-wave) and $+i\gamma_{SV}$ (downgoing *SV*-wave), with:

$$\gamma_P^2 = \frac{\left(G - \sqrt{G^2 - 4H}\right)}{2}$$
$$\gamma_{SV}^2 = \frac{\left(G + \sqrt{G^2 - 4H}\right)}{2}$$

with:

$$G = \frac{1}{C_{33}C_{44}}\left\{\rho\left(C_{33} + C_{44}\right) - p^2\left(C_{11}C_{33} - C_{13}^2 - 2C_{13}C_{44}\right)\right\}$$
$$H = \frac{1}{C_{33}C_{44}}\left(\rho - p^2 C_{11}\right)\left(\rho - p^2 C_{44}\right)$$

1.2 SH Propagation

The two eigenvalues are :
$-i\gamma_{SH}$ (upgoing *SH*-wave) and $+i\gamma_{SH}$ (downgoing *SH*-wave) where:

$$\gamma_{SH}^2 = \frac{\left(\rho - p^2 C_{66}\right)}{C_{44}}$$

2 EIGENVECTORS FOR $\mathbb{A}$

2.1 PSV Propagation

$$\mathbb{D}_{PSV} = \left[b_P^U, b_{SV}^U, b_P^D, b_{SV}^D\right]$$

with

$$b_P^{U,D} = \begin{bmatrix} \gamma_P \\ \pm i\dfrac{\left(-C_{33}\gamma_P^2 - C_{44}p^2 + \rho\right)}{p\left(C_{13} + C_{44}\right)} \\ \pm i\dfrac{\left(-C_{33}C_{44}\gamma_P^2 + C_{13}C_{44}p^2 - C_{13}\rho\right)}{\left(C_{13} + C_{44}\right)} \\ \dfrac{C_{44}\gamma_P\left(-C_{33}\gamma_P^2 + C_{13}p^2 + \rho\right)}{p\left(C_{13} + C_{44}\right)} \end{bmatrix}$$

$$b_{SV}^{U,D} = \begin{bmatrix} p \\ \pm i\dfrac{\left(-C_{33}\gamma_{SV}^2 - C_{44}p^2 + \rho\right)}{\gamma_{SV}\left(C_{13} + C_{44}\right)} \\ \pm i\dfrac{p\left(-C_{33}C_{44}\gamma_{SV}^2 + C_{13}C_{44}p^2 - C_{13}\rho\right)}{\gamma_{SV}\left(C_{13} + C_{44}\right)} \\ \dfrac{C_{44}\left(-C_{33}\gamma_{SV}^2 + C_{13}p^2 + \rho\right)}{\left(C_{13} + C_{44}\right)} \end{bmatrix}$$

2.2 Propagation SH

$$\mathbb{D}_{SH} = \left[b_{SH}^U, b_{SH}^D\right] = \sqrt{\frac{1}{2C_{44}\gamma_{SH}}}\begin{bmatrix} 1 & 1 \\ -iC_{44}\gamma_{SH} & iC_{44}\gamma_{SH} \end{bmatrix}$$